Electronic Supplementary Material (ESI) for Physical Chemistry Chemical Physics.

Supplementary information: First-principles calculations of oxygen octahedral distortions in $LaAlO_3/SrTiO_3$ (001) superlattices

L. Wang,[a] W. Pan,[a] D. Han,[a,c] W. X. Hu[b] and D. Y. Sun[a]

[a.] *Department of Physics, East China Normal University, No.500, Dongchuan Road, Shanghai 200241, People's Republic of China*

[b.] *The computer Center, East China Normal University, No.500, Dongchuan Road, Shanghai 200241, People's Republic of China*

[c.] *Department of Chemistry, Ludwig-Maximilians-Universität, München D81377, Germany*

Contents

1. Layer resolved octahedral tilting and rotation angles $LaAlO_3/SrTiO_3$ (LAO/STO) (001) SLs at different in-plane lattice constants

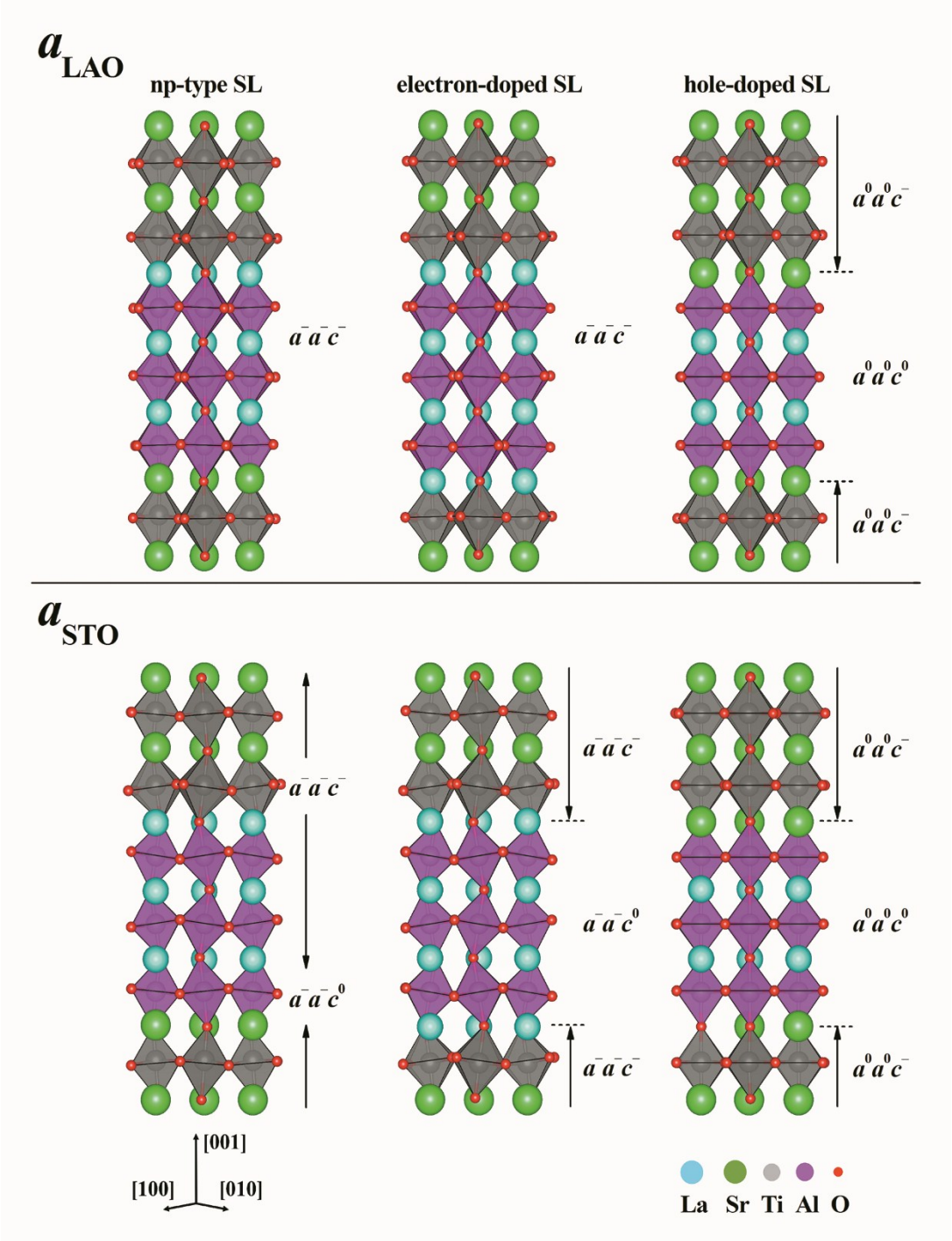

Figure S1. The optimized $LaAlO_3/SrTiO_3$ (LAO/STO) (001) superlattice (SL) geometries viewed along the [110] direction. The top panels show the optimized LAO/STO (001) SLs under compressive strain (the in-plane lattice constant taking

a_{LAO}), the bottom panels show the optimized LAO/STO (001) SLs under tensile strain (the in-plane lattice constant taking a_{STO}). Gray and purple octahedron are centered around Ti and Al ions, respectively.

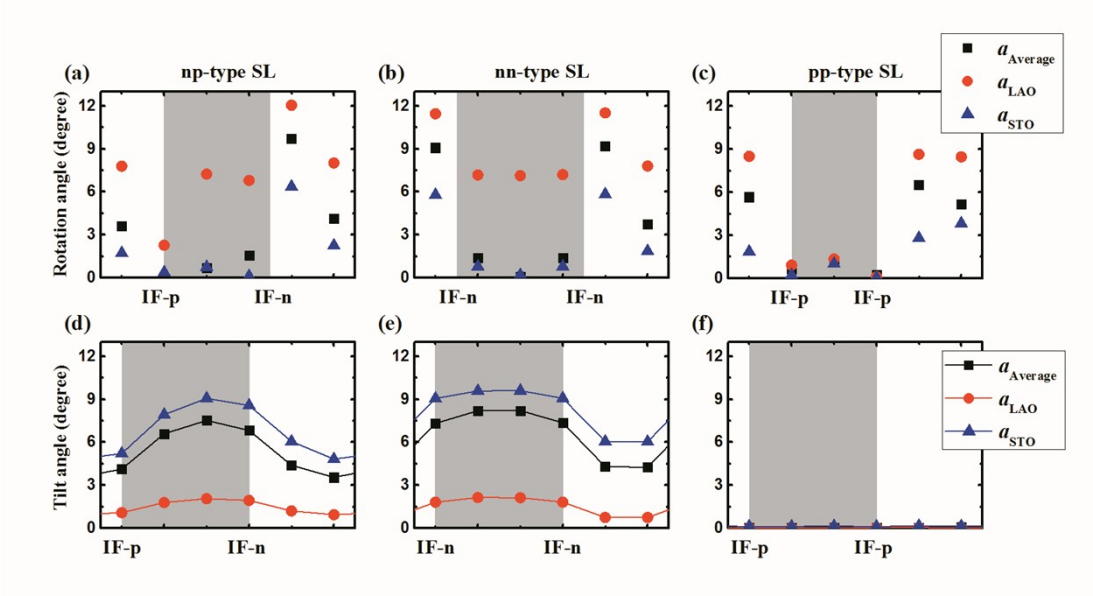

Figure S2. Layer-resolved oxygen octahedral rotation angles **Ω** for the np-type, the electron-doped and the hole-doped SLs are show in (a), (b) and (c), respectively. (d), (e) and (f) correspond to layer-resolved oxygen octahedral tilt angles **Θ** for the np-type, the electron-doped and the hole-doped SLs, respectively. **Ω** and **Θ** refer to the definitions in Ref. [1]. IF-n and IF-p mark the positions of $(LaO)^{1+}/(TiO_2)^0$ interfaces and $(SrO)^0/(AlO_2)^{1-}$ interfaces, respectively. The white and light gray areas indicate $SrTiO_3$ and $LaAlO_3$ components, respectively. Black squares, red circles and blue triangle represent the results for the in-plane lattice constant taking $a_{Average}$, a_{LAO} and a_{STO}, respectively.

Strain plays an important role in determining the octahedral behavior in perovskite oxides. To explore how the in-plane lattice constant affect final results, additional calculations were then performed in which the in-plane lattice constant was set to the one of LAO (pseudocubic, a_{LAO} = 3.819 Å) or STO (a_{STO} = 3.935 Å), corresponding to

SLs grown on the respective (001) substrate.

Results for a_{STO}, corresponding to an underlying STO (001) substrate. The LAO layer in the LAO/STO (001) SLs at a_{STO} is subjected to a tensile strain. As illustrated in Figure S1, the optimized LAO/STO (001) SLs at a_{STO} showed that the oxygen octahedron tilted in a manner similar to that in LAO/STO (001) SLs at $a_{Average}$. For the np-type and the electron-doped SLs at a_{STO}, the LAO region under biaxial tensile strain exhibits an $a^-a^-c^0$ octahedral tilting pattern, and to maintain the connectivity of the oxygen octahedron across the interface, the $a^-a^-c^0$ OOT distortion in the LAO layer also propagated to the STO layer. Coupled with the $a^0a^0c^-$ octahedral rotation from the strain-free STO layer[2], the STO region exhibited an $a^-a^-c^-$ octahedral rotation pattern.

The $a^-a^-c^0$ octahedral tilting distortion in the hole-doped SL at a_{STO} is completely inhibited, while the STO region exhibited an $a^0a^0c^-$ octahedral rotation pattern (Figure S2 [c] and [f]). On the basis of the concept of Goldschmidt tolerance factor[3], the suppression of OOT in the hole-doped LAO/STO (001) SL a_{STO} can be explained by hole-doping effects. According to the ratio of the AO square, a, and the BO_2 square, a □, the Goldschmidt tolerance factor, t, of ABO_3 perovskite oxides is defined as follows:

$$t = \frac{a}{a□} = \frac{r_A + r_O}{\sqrt{2}(r_B + r_O)} = \frac{1}{\sqrt{2}}(1 + \frac{r_A - r_B}{r_B + r_O}) \quad (1)$$

where r_A, r_B and r_O are the ionic radii of A-site, B-site (B = Ti, Al), and oxygen ions, respectively. Holes captured at the p_y (p_x) of the oxygen atoms in the LaO layers and the p_z orbitals of the oxygen atoms in the AlO_2 layers along the [100] crystal orientation ([010] crystal orientation), resulting in a decrease in the radii of corresponding oxygen

ions. On the basis of Equation (1), and the radius of La^{3+} is larger than that of Al^{3+}, the decrease in the radii of oxygen ions results in the increase in *t*. Since the rotation of oxygen octahedron along the [100] ([010]) axis was suppressed, the tilting distortion of oxygen octahedron in the LAO layer disappeared.

Results for a_{LAO}, corresponding to an underlying LAO (001) substrate. The STO layer in the LAO/STO (001) SLs at a_{LAO} is subjected to a compressive strain. As illustrated in Figure S1, top panels, the LAO layer in the np-type or the electron-doped LAO/STO (001) SLs at a_{LAO} exhibites an $a^-a^-c^-$ octahedral rotation pattern different from the corresponding cases at $a_{Average}$ or a_{STO}. This result is consistent with theoretical calculations which suggested that, due to clamping effect of a substrate at very small strains of – 0.2 to 0.1 %, the ground state of LAO is *C*2/*c* ($a^-a^-c^-$ in Glazer notation).[4] To maintain the connectivity of the oxygen octahedron across the interface, the rotation of oxygen octahedron along the [100] ([010]) axis also propagated to the STO layer. Coupled with the $a^0a^0c^-$ oxygen octahedral rotation pattern from the STO layer under compressive strain[5], the STO region exhibited an $a^-a^-c^-$ ochtahedral rotaion pattern in the np-type or the electron-doped LAO/STO (001) SLs at a_{LAO}.

As illustrated in S2 (c) and (f), the $a^-a^-c^-$ octahedral tilting distortion in the LAO region in the hole-doped SL at a_{LAO} is significantly suppressed. Meanwhile, there is an obvious biaxial compressive strain caused OOR in the STO region with $\mathbf{\Omega} \sim 9^\circ$. On the basis of Equation (1), holes captured at the p_y (p_x) orbital of the oxygen atoms in the LaO layers and the p_z orbital of the oxygen atoms in the AlO_2 layers along the [100] crystal orientation ([010] crystal orientation), resulting in a suppression of BO_6

octahedron rotation about the [100] crystal orientation ([010] crystal orientation). While holes captured at the p_x and p_y orbtials of the oxygen atoms in the AlO_2 layers, leading to a suppression of BO_6 octahedron rotation about the [001] crystal orientation. Therefore, due to hole-doing effects, the $a^-a^-c^-$ octahedral tilting distortion in the LAO region in hole-doped SL at a_{LAO} was suppressed.

We found that tensile strain (a_{STO}) induces rotations of oxygen octahedron about the in-plane axes while compressive strain (a_{LAO}) induces rotations of oxygen octahedron about the *c*-axis, as shown in Figure S2. This effect can be attributed to the epitaxial constraint contracts (elongates) the equatorial bond lengths and elongates (contracts) the apical bonds under compressive (tensile) strain.[6]

Based on above mentioned results, the appearance of multiple types of octahedral rotation patterns in SLs at a_{STO} and a_{LAO} can also be explained by the interplay of epitaxial strain, interfacial oxygen octahedral coupling and hole-doping effects. Consequently, we posited that the selection of in-plane lattice parameter will not affect the general validity of our conclusions.

2. Metal-insulator transition in electron-doped $(LAO)_{4.5}/(STO)_{1.5}$ (001) SL

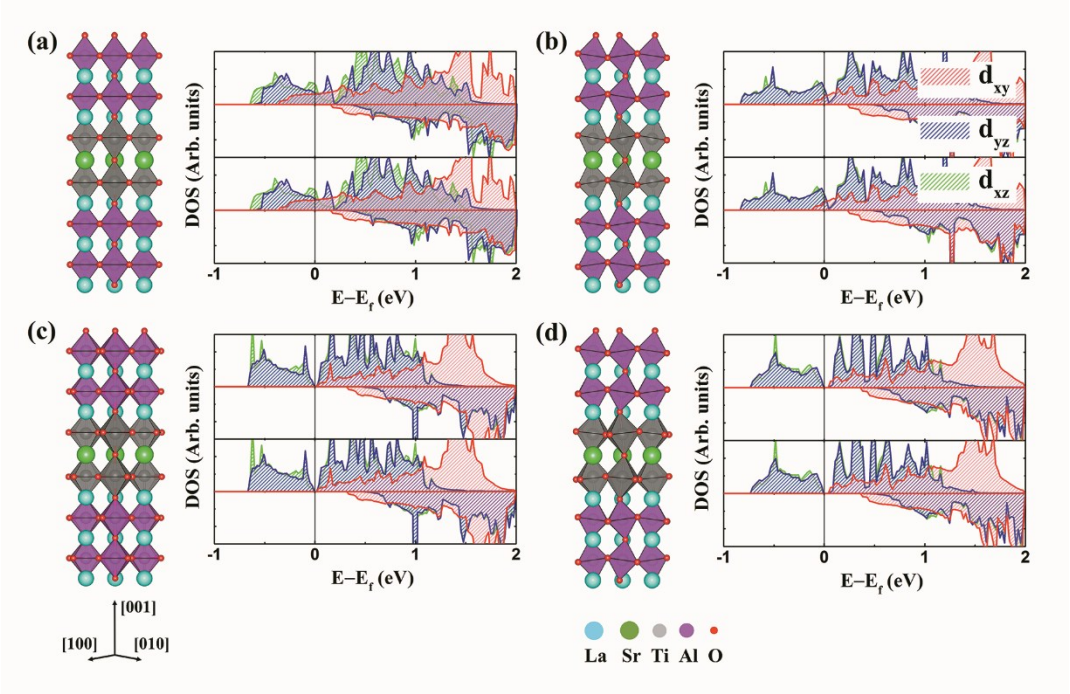

Figure S3. (Color online) Side views of the electron-doped $(LAO)_{1.5}/(STO)_{1.5}$ (001) SL geometries considered herein: (a) with no octahedral rotation distortion, (b) with $a^-a^-c^0$ octahedral tilting distortion, (c) with $a^0a^0c^-$ octahedral rotation distortion, and (d) fully optimized $(LAO)_{4.5}/(STO)/_{1.5}$ (001) with the Ti-3d orbital-resolved density of states.

Experimental and theoretical studies proposed that, with the decrease of STO quantum well thickness in the $GdTiO_3$/STO or electron-doped LAO/STO heterostructure, the system transforms from metal to Mott insulator[7-9]. As illustrated in Figure S3 (d), the optimized $(LAO)_{4.5}/(STO)_{1.5}$(001) superlattice is indeed an insulator. We compared three electron-doped $(LAO)_{4.5}/(STO)_{1.5}$(001) SLs: (1) a system without oxygen octahedral distortions (Figure S3 [a]); (2) a system including $a^-a^-c^0$ octahedral tilting distortion (Figure S3 [b]); and (3) a system containing $a^0a^0c^-$ octahedral rotation distortion (Figure S3 [c]). According to the corresponding DOS of each system shown in Figure S3, it can be seen that the structure, either without oxygen

octahedral distortion or only containing $a^{-}a^{-}c^{0}$ OOT distortion, is still metallic. However, the system containing $a^{0}a^{0}c^{-}$ octahedral rotation distortion is transformed into an insulator. Based on the above results, we confirmed that the $a^{0}a^{0}c^{-}$ octahedral rotation distortion is the key factor responsible for transformation into a Mott insulator in the electron-doped LAO/STO(001) heterointerface.

3. Layer-resolved partial density of states (LDOS) for the hole-doped SL.

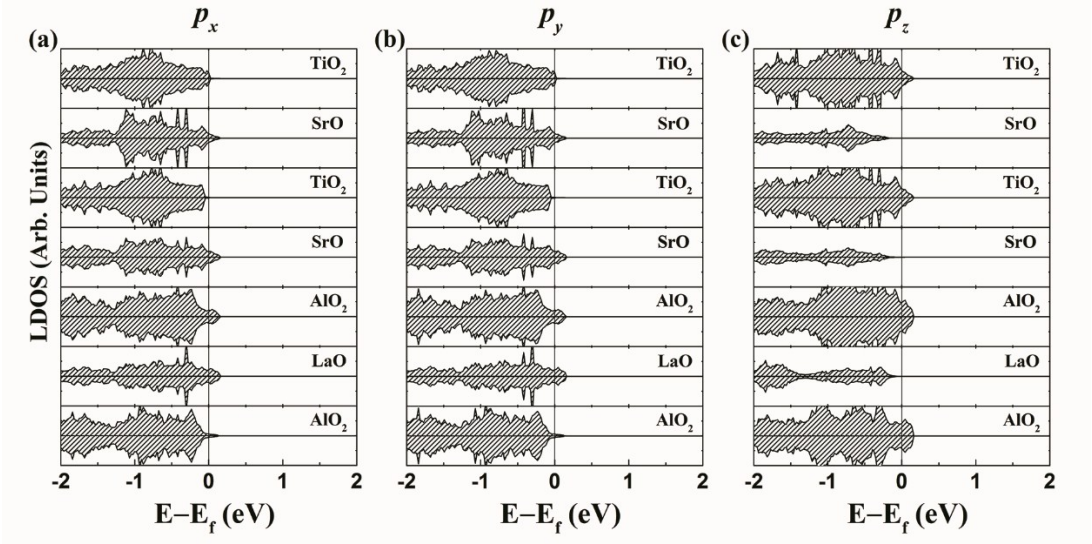

Figure S4. Layer-resolved partial density of states (LDOS) for the hole-doped SL. Only half of the layers are shown due to the inversion symmetry of the SL.

4. Layer-resolved polar distortions of $LaAlO_3/SrTiO_3$ (LAO/STO) (001) SLs

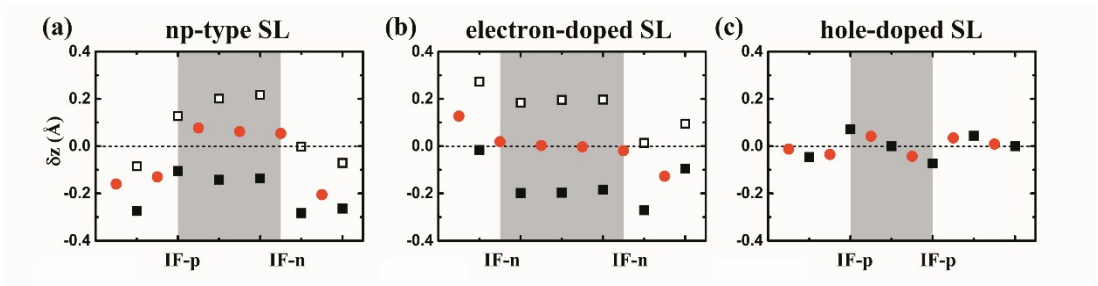

Figure S5. Layer-resolved polar distortions of (a) the np-type, (b) electron-doped and (c) hole-doped $LaAlO_3/SrTiO_3$ (001) SLs. Red circles denote displacement of the oxygen atoms with respect to the neighboring cations in AO (A = La, Sr) layers, while hollow squares and solid squares denote the relative displacement in BO_2 (B = Al, Ti) layers, which correspond to the upward and downward shifts, respectively.

5. Lattice constants and the rotation angle for the *I*4/*mcm* phase of STO.

Table S1. Lattice constants (*a* and *c*) and the rotation angle (**Ω**) for the *I*4/*mcm* phase of $SrTiO_3$. Experimental data are collected from Ref. [10]. Values obtained with the HSE06 hybrid functional are from Ref. [11].

	*I*4/*mcm*			
	GGA + U	PBE	HSE	Experiment
a (Å)	3.960	3.935	3.902	3.898
c / *a*	1.008	1.005	1.001	1.001
Ω (°)	7.0	5.0	2.0	2.1

Using GGA + U and PBE approaches, the structural parameters for a pure STO in *I*4/*mcm* phase are evaluated, given in Table S1. Our results show that the structural parameters and TiO_6 octahedron rotation angle obtained by GGA + U and PBE both larger than the experimental values. The calculated PBE results give better agreement with the experimental data than dose GGA + U. As shown in Table S1, the HSE06 hybrid functional reproduces the structural parameters very accurately. However, using hybrid functional approaches, the structure optimization of supercell requires enormous computational time. This is beyond our current computational facilities. Therefore, most calculations described in this paper were carried out using the PBE functional. However, to study which kind of lattice distortion responds to the Mott transition in electron-doped LAO/STO (001) superlattices, the GGA + U method was adopted.

References

[1]A. T. Zayak, X. Huang, J. B. Neaton, and K. M. Rabe, *Phys. Rev. B*, 2006, **74**,

094104.

[2]G. Shirane and Y. Yamada, *Phys. Rev.* 1969, **177**, 858.

[3]V. M. Goldschmidt, *Naturwissenschaften*., 1926, **14**, 477-485.

[4]A. J. Hatt and N. A. Spaldin, *Phys. Rev. B*, 2010, **82**, 195402.

[5]Feizhou He, B. O. Wells and S. M. Shapiro, *Phys. Rev. Lett*., 2005, **94**, 176101.

[6]S. J. May, J.-W. Kim, J. M. Rondinelli, E. Karapetrova, N. A. Spaldin, A. Bhattacharya, and P. J. Ryan, *Phys*. *Rev*. *B*, 2010, **82**, 014110.

[7]P. Moetakef, C. A. Jackson, J. Hwang, L. Balents, S. J. Allen, and S. Stemmer, *Phys. Rev. B*, 2012, **86**, 201102.

[8]J. Y. Zhang, C. A. Jackson, R. Chen, S. Raghavan, P. Moetakef, L. Balents, and S. Stemmer, *Phys. Rev. B*, 2014, **89**, 075140.

[9]L. Bjaalie, A. Janotti, B. Himmetoglu, and C. G. Van de Walle, *Phys. Rev. B*, 2014, **90**, 195117.

[10]A. Erba, Kh. E. El-Kelany, M. Ferrero, I. Baraille, and M. Rérat *Phys. Rev. B*, 2013, **88**, 035102.

[11]M. Choi, F. Oba, Y. Kumagai, and I. Tanaka, *Adv. Mater.*, 2013, **25**, 86–90.